

Chapter 5

Quasicrystalline Epitaxial Single-Element Films

Adsorption of different elements and molecules on quasicrystals has been the topic of experimental research for several years. The question whether quasicrystal surfaces could be used as templates for a single kind of atom or molecule to adapt the quasicrystalline symmetries has been under intense consideration. The interest in such systems arises from basic properties related to quasicrystals. The question whether the complex alloy composition or the aperiodic structure itself is responsible for the unusual properties of quasicrystals has not been solved yet. A possible approach to resolve this problem is the growth of single element quasicrystals. Such quasicrystals have not been found and it has been argued that there might be fundamental reasons for bulk quasicrystals of one species only not to exist. This is explained by the impossibility to adjust the valence electron to atom ratio e/a with a single element such that the electronic states are occupied up to a symmetry derived pseudo-gap. It might, however, be possible to stabilize the quasicrystalline structure in a single element film by a quasicrystalline substrate.

In an effort to find a possible candidate for such an adsorbate system, several kinds of atoms and molecules have been deposited on the tenfold surface of decagonal (d) Al-Ni-Co and the fivefold surface of icosahedral (i) Al-Pd-Mn. In these studies, preferential adsorption sites have been found for submonolayer coverages, but whenever the coverage of a closed layer was approached the result was a disordered adsorbate structure [10-13].

Deposition of gold (Au), platinum (Pt), aluminum (Al), and silver (Ag), on the other hand, has demonstrated that a long-range order can indeed exist in closed surface coverages, but not as a quasicrystalline structure. These films exhibit the rotational symmetry of the substrate by consisting of multiply twinned domains of periodic atomic structure [9, 14-16, 109, 110].

The only reports at all of epitaxial quasicrystalline films with long-range order on a qua-

quasicrystal regard alloyed layers on the fivefold Al-Pd-Mn surface, which have been obtained by ion bombardment and annealing of the substrate. While Bolliger et al. reported a thin film (20 Å) of $\text{Al}_{22}\text{Pd}_{56}\text{Mn}_{22}$ [17], Naumovic et al. observed a surface layer of several Ångström thickness consisting of the stable decagonal $\text{Al}_{69.8}\text{Pd}_{12.1}\text{Mn}_{18.1}$ bulk phase [18].

Hence, it still remained unresolved whether a single element can form a quasicrystalline two-dimensional overlayer. In this chapter, the formation of quasicrystalline ultra-thin Bi and Sb films on the fivefold surface of icosahedral-Al-Pd-Mn and the tenfold surface of decagonal-Al-Ni-Co, has been investigated. The adsorption process as monitored by HAS will be presented first. The structure of the monolayer coverage will then be resolved by elastic helium and electron diffraction.

5.1 Adsorption Process

The film growth of Sb and Bi on the fivefold surface of i-Al-Pd-Mn and on the tenfold surface of d-Al-Ni-Co was studied by monitoring the intensity of the specular He atom beam during deposition at constant adsorbate flux as shown in figures 5.4 (a) and 5.5 (a). Due to the large cross section for diffuse scattering of the adsorbates at low coverages, the intensity falls off steeply, passes through a minimum and saturates at a specific coverage. Further adsorption of Sb and Bi leads to a monotonous decrease in He intensity.

However, the detailed shape depends significantly on the beam energy as well as the sample temperature. For example, an exponential decrease of the specular intensity is expected for a random adsorbate distribution while island formation yields a linear decay [54]. The encountered adsorbate distribution results from the atomic processes on the surface, such as diffusion, interaction between the adsorbates and desorption. A high mobility of the adsorbates at elevated temperatures allows them to diffuse and saturate step edges and defects or to form islands. Layer growth occurs if the diffusion coefficient of adsorbates in higher layers is sufficiently large to allow the atoms to find vacancies in the underlying layer and saturate these. Moreover, a difference in He beam energy yields different scattering phases between adsorbate and substrate, thus also leading to a variation in the shape of the deposition curve. However, the cross section of a specific adatom is practically independent of the respective substrate [45].

A simulation of the adsorption curves can give evidence of the underlying growth mode. In addition, it can serve as a tool to calibrate the coverage for which it is used here. In a first step, the scattering cross section of Sb and Bi will be derived from a system where the monolayer coverage is known. For this, the III-V semiconductor surface GaAs(110) was chosen, on which Sb and Bi form an epitaxially continued monolayer [51, 111]. Then the adsorption curves of Sb

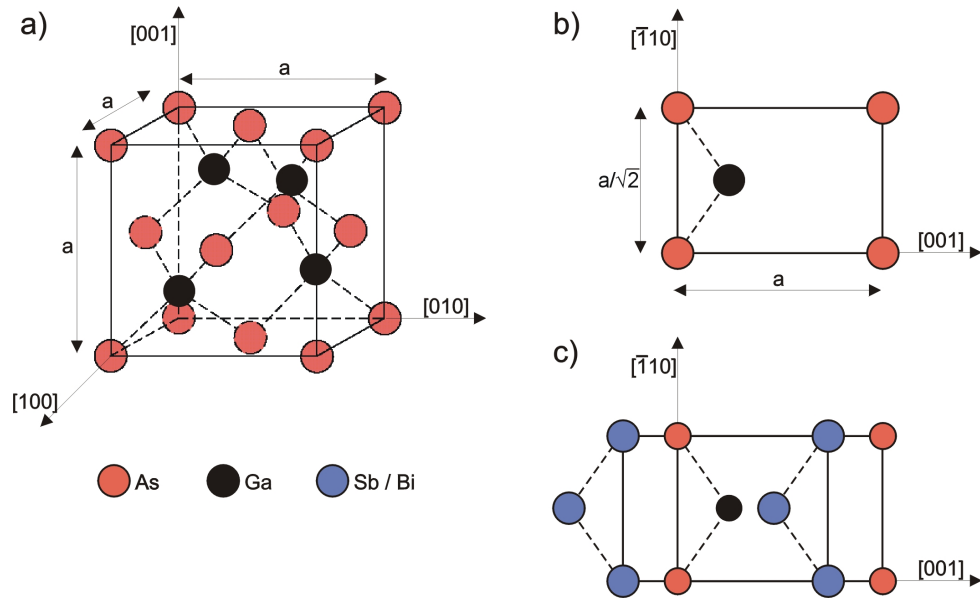


Figure 5.1: Schematic sphere model of the zinc-blende structure encountered in GaAs. (a) shows the volume unit cell, while (b) depicts the (110) surface unit cell, (c) is a schematic of the epitaxially continued layer structure of the Sb/Bi monolayer.

and Bi on the quasicrystal surfaces are modeled with the same scattering cross sections.

5.1.1 Coverage Determination

Before presenting the details of the adsorption curve analysis, a brief introduction into the structure of GaAs (110) and the Bi and Sb monolayers on that surface is given.

Structure of GaAs (110) and Bi/Sb monolayers on GaAs (110)

GaAs crystallizes in the zinc-blende structure of lattice parameter $a = 5.653 \text{ \AA}$ [112]. The structure can be regarded as two cubic face centered lattices of Ga and As shifted by a quarter of a volume diagonal with respect to each other. Each atom is therefore surrounded by four nearest neighbors of the contrary species.

The (110) -plane consists to equal amounts of the two atomic species. It has been shown by several experimental and theoretical studies that the surface As atoms undergo an inward and the Ga atoms an outward relaxation [113]. The reason for this relaxation can be found in the existence of dangling bonds at the surface due to a missing nearest neighbor. The bulk sp_3 -hybridization is canceled in favor of three sp_2 -configurations of the Ga atoms and one p -orbital filled with two electrons of the more electronegative As atoms, such that all bonds are saturated

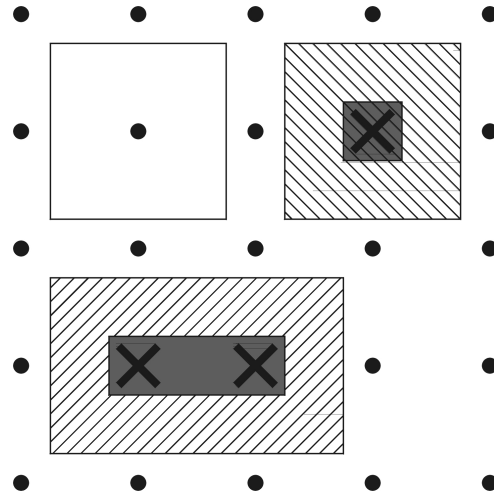


Figure 5.2: Illustration of scattering contributions to the He specular intensity from a partly covered surface. Sites occupied by adsorbates are marked by crosses. The scattering area corresponding to a specific site is marked by a square. The dashed areas scatter diffusely while the white and dark gray areas contribute with a different reflectivity to the specular He intensity.

[114]. As can be seen from figure 5.1(b), the $[\bar{1}10]$ -direction can be described as a zig-zag chain of alternating Ga and As atoms.

While Sb forms a perfect epitaxially continued monolayer on GaAs [115], the larger covalent radius of the Bi atoms induces defects, i.e., vacancies, along the zig-zag chains. On average, after every 13 atoms one Bi atom is missing [116]. Perpendicular to these chains no change in periodicity is observed. With a surface unit cell area of 22.597 \AA^2 , two atoms per unit cell and the defect density discussed above, the densities of the Sb and Bi atoms on GaAs(110) amount to $0.85 \times 10^{-15} \text{ cm}^{-2}$ and $0.82 \times 10^{-15} \text{ cm}^{-2}$, respectively.

Calibration of the Adsorption Curves on the Quasicrystal Surfaces

In the first step to determine the coverage of Bi and Sb on the quasicrystal surfaces the specular intensity from the reference system Bi and Sb on GaAs(110) is modeled. The model incorporates the atomic distribution of the adsorbates on a rectangular substrate lattice with 10000 sites. In each simulation step a selectable number of atoms, representing the flux from the evaporator, are incident on random sites of the substrate. The adsorbed atoms can diffuse on the substrate or desorb. Both the diffusion and desorption probability can be adjusted by parameters which differ for adsorbates directly on the substrate and on higher adsorbate layers. The diffusion can additionally be controlled by a parameter governing the attraction between the adsorbates.

After such a step simulating the atomic processes on the surface, the reflected He intensity is

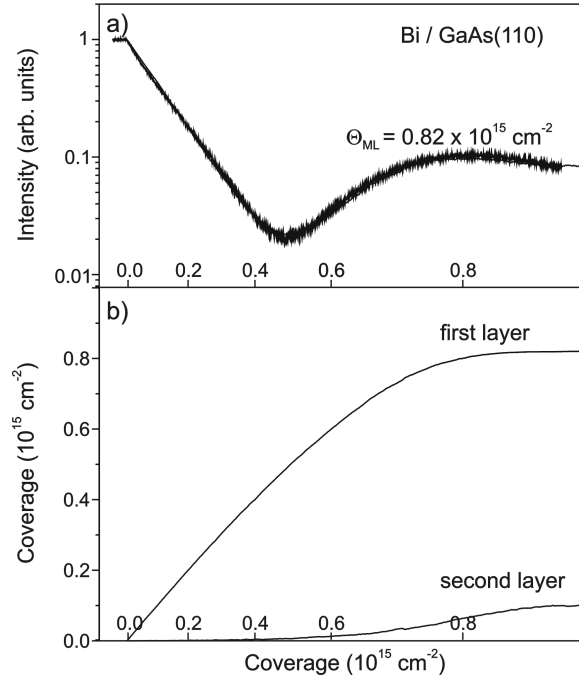


Figure 5.3: Deposition curves of Bi on a cleaved GaAs(110) surface. (a) Specular He intensity from experiment (thick line) and simulation (thin line). The experimental curve was recorded at 15 meV He beam energy and 20 °C sample temperature. (b) Coverage in the first and second layer in the simulation.

calculated, following the model of Poelsema and Comsa [54]. For this, each atom of the topmost surface layer is associated to an area which contributes to the intensity. In good approximation, the area can be chosen to have the same symmetry as the substrate lattice [54] as indicated in figure 5.2. Both the size of this area and its reflectivity are determined by a separate parameter. While the area corresponding to substrate and adsorbate atoms is equivalent, their reflectivity parameter is independent from each other. Additionally, a phase factor $e^{i\phi}$ is associated with higher adsorbate layers. In order to determine the He intensity, the precise distribution of the adatoms on the surface is required. If scattering areas of atoms in different surface layers overlap, the overlapping area produces diffuse scattering and thus does not contribute to the specular intensity. Areas with no overlap or overlap of cross sections from the same layer are weighted by their corresponding reflectivity and phase factor. The calculation of the scattering areas is illustrated in figure 5.2. The He intensity is then given by

$$I_{spec} = \left| \sum_n SA_n r_n e^{i\phi_n} \right|^2 \quad (5.1)$$

with the sum over layers n and SA_n the scattering areas, r_n their reflectivities, and ϕ_n the

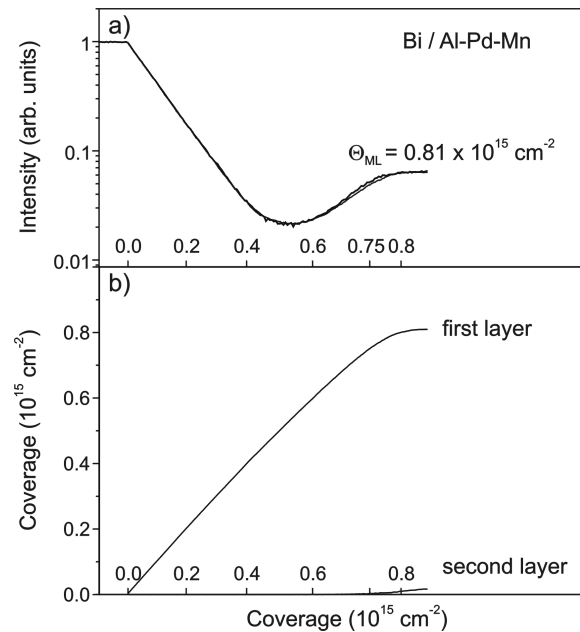


Figure 5.4: Deposition curves of Bi on the fivefold surface of Al-Pd-Mn. (a) Specular He intensity from experiment (thick line) and simulation (thin line). The experimental curve was recorded at 15 meV He beam energy and 150 °C sample temperature. (b) Coverage in the first and second layer in the simulation.

corresponding phase factors. The process just described is repeated a few hundred times to complete the adsorption curve.

By fitting all the introduced parameters, the adsorption curve can be simulated as shown in figure 5.3 (a) for Bi on GaAs(110). For the figure a curve was chosen whose initial decrease in intensity follows an exponential decay. From this a random distribution of the adsorbates and therefore a limited diffusion on the substrate can be deduced. However, the diffusion barrier in higher layers is considerably lower, as an almost perfect layer growth can be inferred from the strong increase in intensity at larger coverages. With the known coverage of $0.82 \times 10^{-15} \text{ cm}^{-2}$ in the first monolayer, the resulting evolution of the coverage in the first and second layer can be determined from the simulation as indicated in figure 5.3 (b).

The cross section for diffuse scattering of Bi at specific He beam energies can then be derived from the decrease in intensity associated with a single adatom. This corresponds to the initial slope of the normalized He intensity curve. As mentioned previously, the scattering cross section for a specific adsorbate at a specific energy is constant such that the corresponding adsorption curves on the quasicrystal surfaces can be rescaled along the x -axis to yield identical slopes.

An equivalent growth modeling procedure is then applied to simulate the adsorption curves

on the quasicrystal surfaces. For Bi and Sb on the fivefold surface of Al-Pd-Mn this yields a monolayer coverage of $(0.8 \pm 0.2) \times 10^{-15} \text{cm}^{-2}$. The error has been estimated by comparison of two slightly different models, deviations of fit parameters and the simplifications used in the model. The diffusivity of atoms in the first layer under these experimental conditions (150°C) is sufficiently low to rule out island formation or the saturation of defects or step edges as revealed by the exponential decrease in He intensity at low coverage. On the other hand, the diffusion probability for atoms in higher layers was found to be very large, leading to a completion of the first monolayer before the second layer starts to grow. This is represented by the evolution of the coverage in the first and second layer as indicated in figure 5.4 (b).

In contrast, the tenfold Al-Ni-Co sample had to be cooled to -50°C in order to limit diffusion in the first layer. This different behavior on the quasicrystalline surfaces can be explained by the lower corrugation of the tenfold surface of Al-Ni-Co with respect to the Al-Pd-Mn surface. (The relation of the corrugation is discussed in section 5.3.3). However, the cooling also leads to a decrease of the diffusion in higher layers. This is demonstrated by the resulting coverage in the first and second layer in figure 5.5 (b). The calibration of the coverage yields a monolayer

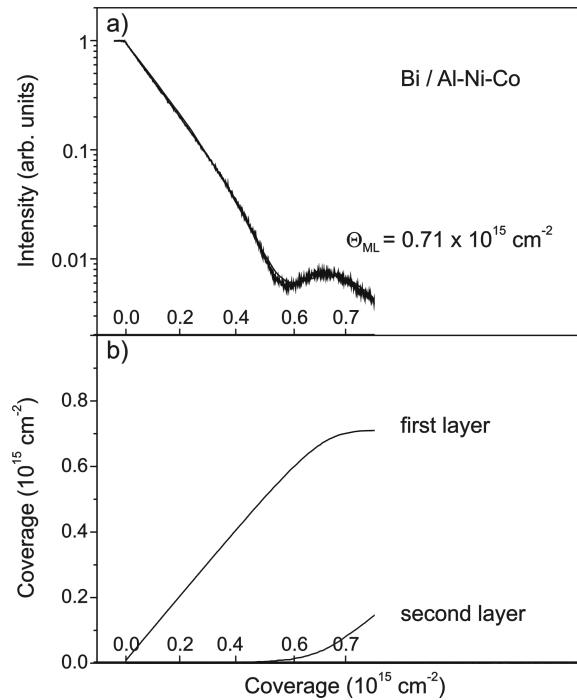


Figure 5.5: Deposition curves of Bi on the tenfold surface of Al-Ni-Co. (a) Specular He intensity from experiment (thick line) and simulation (thin line). The experimental curve was recorded at 15 meV He beam energy and -50°C sample temperature. (b) Coverage in the first and second layer in the simulation.

Desorption temperature	Quasicrystals	GaAs(110) [111]
Bi monolayer	(400 – 600)°C	270°C
Bi multilayer	(150 – 250)°C	(150 – 250)°C
Sb monolayer	(700 – 750)°C	550°C
Sb multilayer	(150 – 350)°C	(200 – 350)°C

Table 5.1: Desorption temperatures of the Sb and Bi mono- and multilayers on the tenfold surface of d-Al-Ni-Co and the fivefold surface of i-Al-Pd-Mn in comparison to GaAs(110)

of $(0.7 \pm 0.2) \times 10^{-15} \text{cm}^{-2}$ for both Bi and Sb on this surface.

5.2 Thermal Stability

In order to examine the thermal stability of the Sb and Bi mono- and multilayers on the sample surface, the He specular intensity was monitored. Due to an increased Debye-Waller attenuation at high temperatures the specular intensity decreases with temperature even without changes in Sb or Bi coverage. Therefore, in order to investigate the stability at a specific temperature, the sample was heated to this temperature and subsequently cooled to room temperature where the He intensities are compared. An increase in intensity indicates the desorption of the majority of the adsorbate atoms. Since the temperature could not be measured very accurately the fairly large temperature ranges give only trends in thermal stability.

It is found that the desorption of the Sb and Bi mono- and multilayers occurs at approximately the same temperatures for d-Al-Ni-Co and i-Al-Pd-Mn substrates. The low desorption temperatures of the multilayers of about 150-250 °C and 150-350 °C for Bi and Sb, respectively, reveal weak bonds between the adsorbate atoms in agreement with vapor pressure data. In contrast, the monolayers are more strongly bound to the substrate as is apparent from the significantly higher desorption temperatures of 400-600 °C and 700-750 °C of the Bi and Sb monolayers, respectively. As the Sb monolayer desorbs at temperatures close to the melting point of Al-Pd-Mn it is impossible to obtain a clean surface by heating alone.

The reported thermal stabilities of the corresponding monolayers on GaAs(110) show a similar trend shifted to slightly lower temperatures. The epitaxial Sb film is stable up to 550 °C, whereas additional layers desorb at 200-350 °C. The respective temperatures for Bi are somewhat lower [111]. Consequently, an even higher stability of the first adlayer is observed in the growth of Sb and Bi on the quasicrystal surfaces. Since the only common feature of the two quasicrystal surfaces is their high Al density, the bonding might be ascribed to a strong covalent

Al-Sb or Al-Bi bond. This is supported by the Sb/Bi coverage corresponding to the Al density on the substrate surface as derived in the previous section. Hence, a strong influence of the Al distribution on the structure of the monolayers is expected, which will be investigated in the following.

Additionally, it should be noted that Sb and Bi monolayers are inert to adsorption of residual gases in the experimental chamber which quickly contaminate the Al-rich clean surfaces. This is a further indication of the saturation of all Al atoms at the surface.

5.3 Structure of the Monolayer Coverage

Having determined the thermal stability of the adsorbate layers, the preparation of Sb and Bi monolayers on the quasicrystalline surfaces is relatively simple. The most convenient approach in an experimental set-up without the capability of recording HAS adsorption curves is to deposit multilayers onto the sample and anneal at temperatures above the desorption temperature of the multilayers but below the onset of monolayer desorption. This procedure guarantees the formation of well-ordered monolayers. Since the suitable temperature range spans more than 300 °C the preparation of the films is unproblematic with respect to the temperature calibration. In order to analyze the structure of the Sb and Bi monolayers on the quasicrystalline surfaces, electron diffraction patterns as well as elastic Helium scattering spectra have been recorded.

5.3.1 Sb/Bi Monolayers on i-Al-Pd-Mn(100000)

LEED patterns of the Sb and Bi monolayers on the fivefold Al-Pd-Mn surface and the clean surface are presented in figure 5.6. The monolayers show a more intense LEED pattern with more diffraction peaks observable at 63 eV electron energy. However, they agree with the strong reciprocal lattice points of the clean surface as can be shown by comparing diffraction patterns of different electron energy. As an example, figure 5.6 (b) shows a pattern at 85 eV with other dominant diffraction spots. A quantitative analysis of the observed diffraction spots in the HAS spectra will show that the peaks can be indexed by the bulk basis vectors. The difference in energy dependence of the electron diffraction patterns of the monolayers arises from the difference in the dynamical form factor of the involved atoms.

While the depicted LEED patterns of the Sb and Bi monolayer in figure 5.6 (c) and (d) suggest a tenfold symmetry, this is not the case as can be verified by varying the electron energy. However, considering the penetration depth of several atomic layers of the electrons, an influence of the substrates' structure and symmetry is always expected. In order to confirm the fivefold instead of a tenfold symmetry as well as the quasicrystalline structure of the monolayer

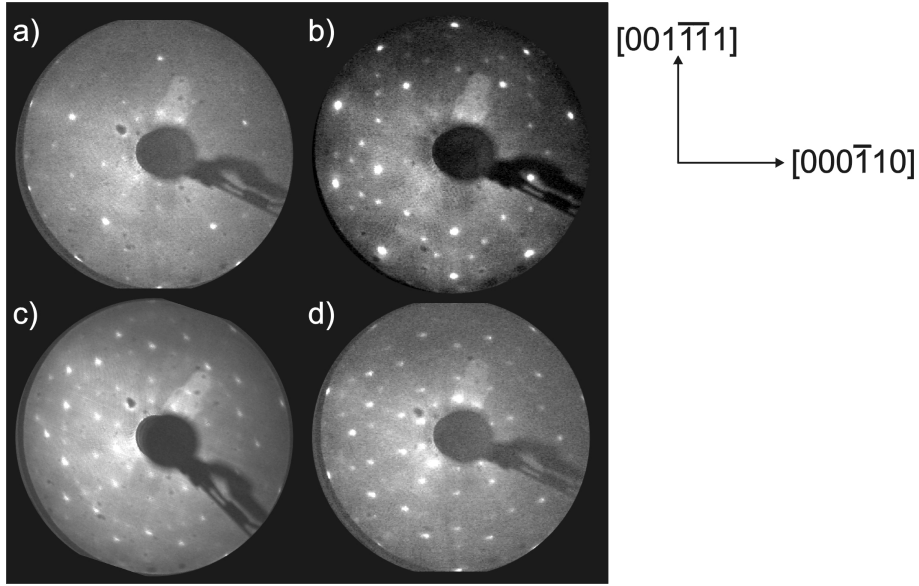


Figure 5.6: LEED images of the clean fivefold Al-Pd-Mn surface recorded with (a) 63 eV, and (b) 85 eV electron kinetic energy. LEED patterns recorded at 63 eV from (c) Sb monolayer, and (d) Bi monolayer on Al-Pd-Mn. Although the LEED patterns of the monolayers might suggest a 10-fold symmetry, they are in fact fivefold as is seen by varying the electron energy.

itself, helium diffraction, being solely sensitive to the topmost layer, is the ideal method.

The diffraction spectra recorded along the high symmetry directions $[001\bar{1}\bar{1}1]$ and $[000\bar{1}10]$, which correspond to the vertical and horizontal of the LEED images in figure 5.6, are shown in figure 5.7. Clearly, all spectra along the $[001\bar{1}\bar{1}1]$ -axis are not mirror symmetric demonstrating that the monolayers do not have a tenfold symmetry. Aside from the diffraction spots at large k_{\parallel} -values the monolayers' diffraction spots coincide with peaks from the clean surface. However, it can be shown that these diffraction spots are also expected for the Al-Pd-Mn surface. The positions of all observed spots are listed in table 5.2. Their relation to the bulk structure of Al-Pd-Mn can be derived from the surface projection of the reciprocal basis vectors introduced in chapter 2. From equation 2.31 these yield

$$P(\mathbf{d}_1^*) = \begin{pmatrix} 0 \\ 0 \end{pmatrix}; P(\mathbf{d}_j^*) = a^* \sin \theta \begin{pmatrix} \cos \frac{2\pi j}{5} \\ \sin \frac{2\pi j}{5} \end{pmatrix} = b^* \begin{pmatrix} \cos \frac{2\pi j}{5} \\ \sin \frac{2\pi j}{5} \end{pmatrix}, j = 2, \dots, 6 \quad (5.2)$$

with $b^* = a^* \sin \theta = 0.99 \text{ \AA}^{-1}$. Since in the surface projection $P(\mathbf{d}_6^*) = -\sum_{h=2}^5 P(\mathbf{d}_h)$, $P(\mathbf{d}_6)$ is not a linearly independent vector and a surface reciprocal vector can be obtained by the linear combination $G = \sum_{j=2}^5 h_j P(\mathbf{d}_j^*)$.

Table 5.2 shows that the diffraction peaks of the Al-Pd-Mn surface are all bulk derived with the peak positions following the characteristic τ -scaling arising from the fivefold symmetry.

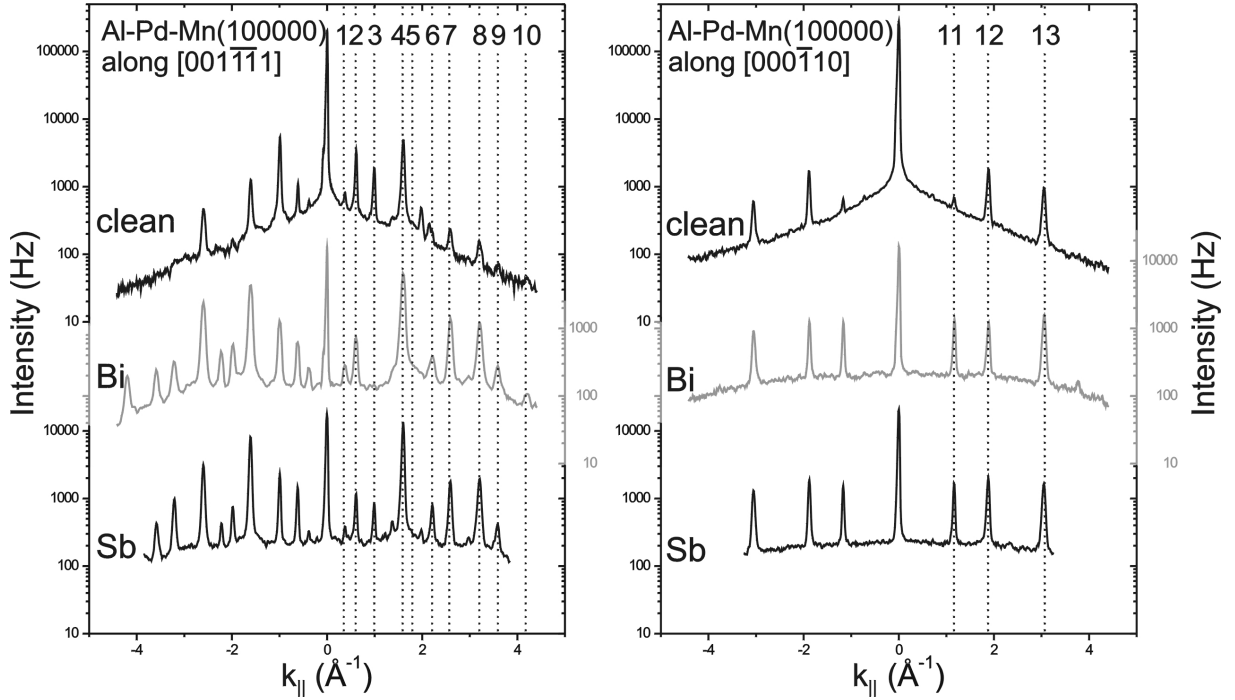


Figure 5.7: He atom diffraction from the clean fivefold Al-Pd-Mn surface and the Sb and Bi monolayers at 15.1 meV He kinetic energy. The left and right column represent the diffraction spectra along the vertical $[001\bar{1}\bar{1}1]$ and horizontal $[000\bar{1}10]$ direction in the LEED pattern of figure 5.6, respectively. The (a,d), (b,e) and (c,f) represent the diffraction from the clean, Bi monolayer and Sb monolayer, respectively.

Moreover, it shows that all diffraction spots of the monolayers agree with those of the clean surface even if they are not observable in those spectra. Consequently, the Sb and Bi monolayers form an epitaxial quasicrystalline film on the Al-Pd-Mn surface. Since the Bragg peaks are very sharp, i.e., the full-width at half-maximum is narrow and limited by the instrumental transfer length, the ordered regions must be larger than 100 Å.

A comparison of the spectra from the monolayers reveals a close similarity in the intensity distribution of the corresponding diffraction peaks. Only the disappearance of the peak at $k_{\parallel} = 0.99 \text{ \AA}^{-1}$ of the Bi monolayer is a striking difference. However, this vanishing is not ascribed to a structural characteristic of the Bi film. At different energies a strong diffraction peak is observed. For the Sb monolayer a similar disappearance of the corresponding spot is found at a slightly different helium beam energy. This is due to a scattering resonance with a bound state in the helium-surface potential.

Spot	$k_{\parallel}/\text{\AA}^{-1}$	$(h_2h_3h_4h_5)$	k_{\parallel}/b^*
1	0.38	(2211)	τ^{-2}
2	0.60	$(\bar{1}0\bar{1}\bar{1})$	τ^{-1}
3	0.99	(1000)	1
4	1.60	$(0\bar{1}0\bar{1})$	τ
5	1.98	(2000)	2
6	2.23	$(\bar{1}0\bar{2}\bar{2})$	$2\tau - 1$
7	2.60	$(\bar{1}0\bar{3}\bar{3})$	τ^2
8	3.19	$(00\bar{2}\bar{2})$	2τ
9	3.60	$(00\bar{3}\bar{3})$	$\tau^2 + 1$
10	4.19	$(\bar{1}\bar{1}\bar{3}\bar{4})$	τ^3
11	1.15	$(01\bar{1}0)$	χ
12	1.88	$(100\bar{1})$	$\chi\tau$
13	3.06	$(11\bar{1}\bar{1})$	$\chi\tau^2$

Table 5.2: Observed diffraction peaks of the Sb and Bi monolayer on the fivefold surface of i-Al-Pd-Mn (see spectra figure 5.7). All spots can be labeled by the surface projected bulk reciprocal basis vectors of Al-Pd-Mn. $\chi = \sqrt{3 - \tau}$ is another characteristic number for fivefold symmetries as it equals the ratio edge to radius in a regular pentagon.

5.3.2 Sb/Bi Monolayers on d-Al-Ni-Co(00001)

In order to investigate the long-range order of the Sb and Bi monolayers on the tenfold surface of decagonal Al-Ni-Co, SPA-LEED patterns were recorded (figure 5.8). The monolayers again exhibit diffraction spots at the same positions as the clean surface with different energy dependence of the intensity. The structure of exclusively the monolayers is studied by helium diffraction. Spectra along the two high symmetry directions $[10000]$ and $[001\bar{1}0]$ are depicted in figure 5.9. Bragg peaks associated with large k_{\parallel} -values are much weaker or even not observable on the clean surface, while for the Sb and Bi monolayers, they reveal relatively high intensities. In order to confirm that these peaks indeed belong to the quasicrystalline structure it is shown that they are indexable with the bulk-derived basis vectors. A compilation of the observed diffraction peaks with their corresponding Miller indices is given in table 5.3. The indexing refers to the basis vectors introduced in section 2.7.2.

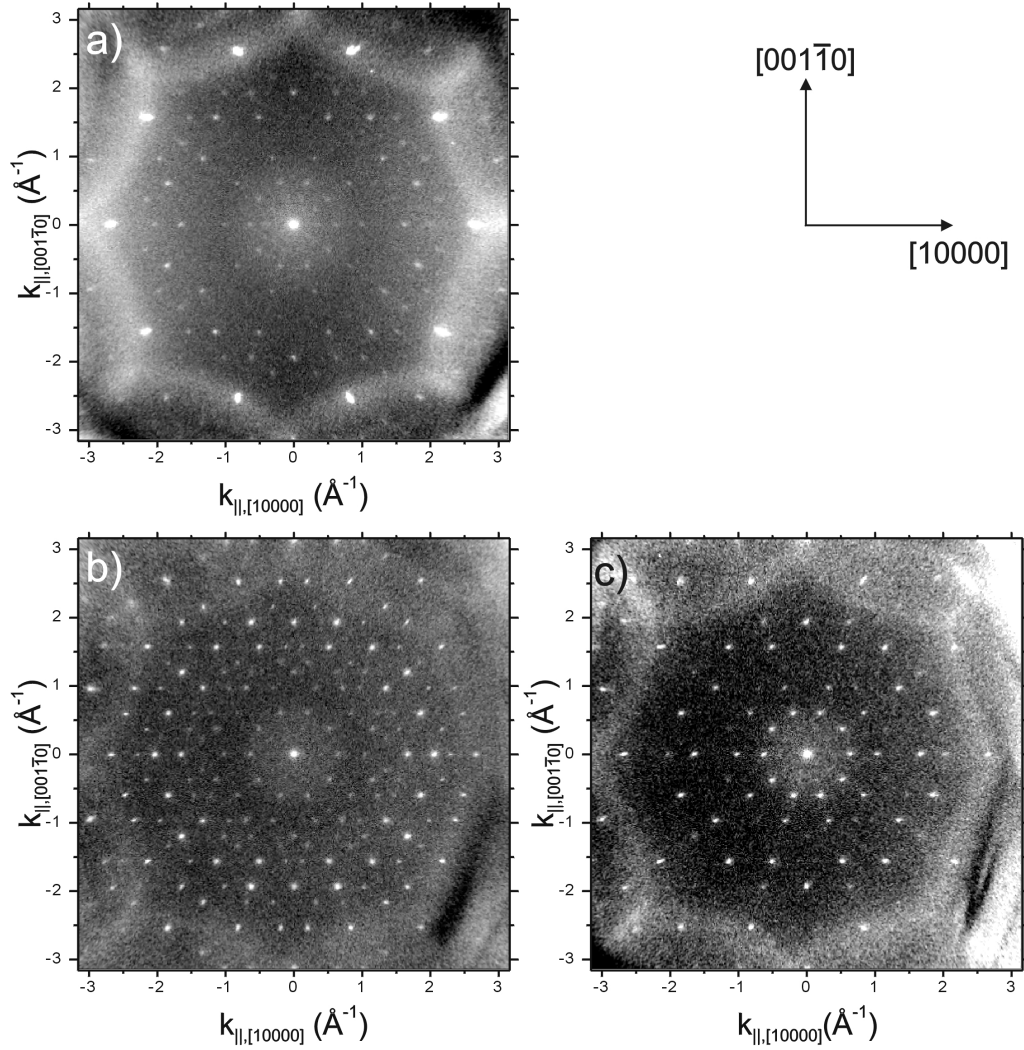


Figure 5.8: SPA-LEED images recorded at 65 eV electron energy from the tenfold Al-Ni-Co surface: (a) clean surface, (b) Sb monolayer, and (c) Bi monolayer.

5.3.3 Corrugation of the Monolayers

The corrugation of the surface can be estimated from the intensity distribution of the HAS diffraction spots. This is due to the fact that a larger corrugation causes more He atoms to be scattered into angles deviating from the specular beam and consequently the intensity of Bragg peaks at larger k_{\parallel} -values increases [45] (see chapter 3.1.3).

In the case of the clean tenfold d-Al-Ni-Co surface, the specular peak dominates the spectra, with all other diffraction spots exhibiting intensities lower by two orders of magnitude. Thus,

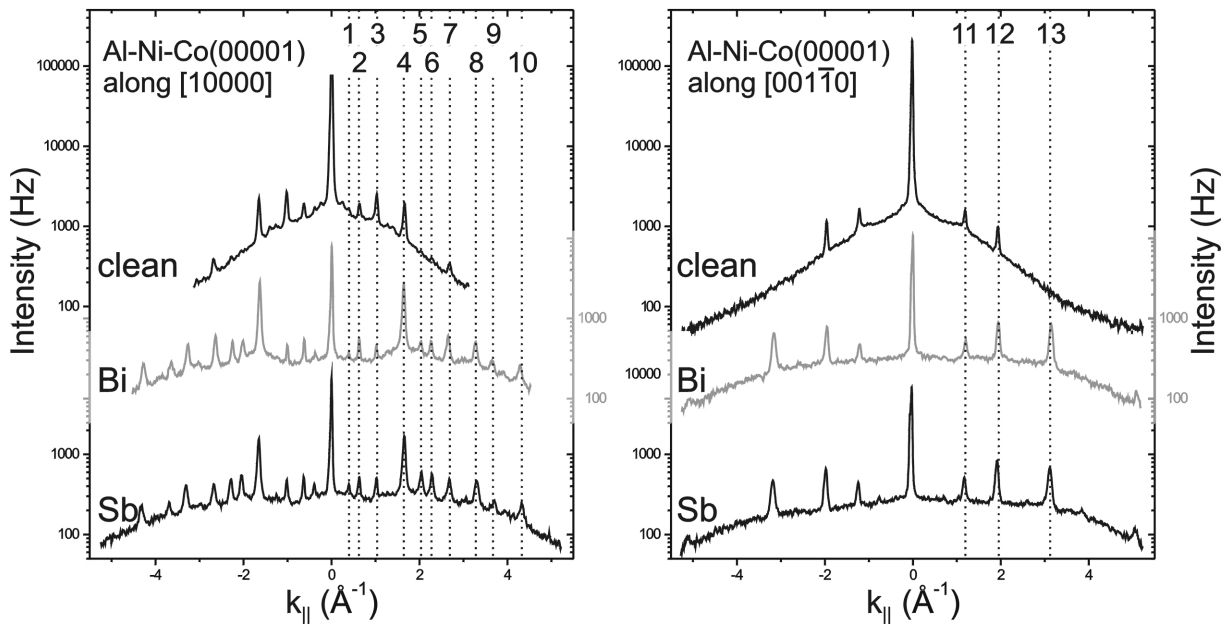


Figure 5.9: He atom diffraction from the clean tenfold Al-Ni-Co(00001) surface and the Sb and Bi monolayers at 21.7 meV He kinetic energy. The left and right column represent the diffraction spectra along the $[00001]$ and $[001\bar{1}0]$ direction, respectively.

a fairly low corrugation can be inferred. This agrees with expectations, as a bulk truncation yields the tenfold planes as terminating terraces (figure 4.10, and [11, 13, 77]).

In contrast, the clean fivefold Al-Pd-Mn(100000) surface exhibits a stronger corrugation as revealed by a larger ratio of Bragg peak to specular intensity. This is also in agreement with possible bulk truncations: In icosahedral quasicrystals the atoms are not located on flat planes [117]. However, it has been shown that the atoms can be grouped into planes parallel to the fivefold surface of varying density and roughness [118, 119]. Of these, buckled layers in which about one third of the atoms is retracted by 0.4 \AA represent the experimentally determined surface termination [67, 68].

Now consider the intensity distribution in the spectra from the monolayers. They all possess the common feature that the intensity of the Bragg peaks does not decay rapidly with momentum transfer. Hence, the Sb and Bi monolayers on both the tenfold Al-Ni-Co(00001) and the fivefold Al-Pd-Mn(100000) surface are more strongly corrugated than the respective substrates. On Al-Pd-Mn the monolayers are significantly more corrugated than on Al-Ni-Co as might be expected on a more corrugated surface.

The implications of the larger corrugation are not unambiguous. While strong covalent bonds to the surface already might lead to a more pronounced corrugation, a buckling of the

Spot	$k_{\parallel}/\text{\AA}^{-1}$	$(h_1h_2h_3h_4)$	k_{\parallel}/b^*
1	0.38	(2211)	$2 - \tau$
2	0.63	$(\bar{1}0\bar{1}\bar{1})$	$1 - \tau$
3	1.02	(1000)	1
4	1.65	$(0\bar{1}0\bar{1})$	τ
5	2.04	(2000)	2
6	2.28	$(\bar{1}0\bar{2}\bar{2})$	$2\tau - 1$
7	2.67	$(\bar{1}0\bar{3}\bar{3})$	$\tau + 1$
8	3.30	$(00\bar{2}\bar{2})$	2τ
9	3.69	$(00\bar{3}\bar{3})$	$\tau + 2$
10	4.32	$(\bar{1}\bar{1}\bar{3}\bar{4})$	$2\tau + 1$
11	1.20	$(01\bar{1}0)$	χ
12	1.94	$(100\bar{1})$	$\chi\tau$
13	3.14	$(11\bar{1}\bar{1})$	$\chi\tau^2$

Table 5.3: Observed diffraction peaks of the clean Al-Ni-Co(00001) surface and the Sb and Bi monolayers (see spectra figure 5.9). All spots can be indexed by the surface projected bulk reciprocal basis vectors of d-Al-Ni-Co.

monolayer would additionally increase the corrugation. A hint to the origin of the corrugation is given by the dominant Bragg point at $k_{\parallel} = \pm 1.65 \text{\AA}^{-1}$ in the diffraction spectra along the [10000]-axis of Al-Ni-Co. This peak corresponds to a modulation of $2\pi/k_{\parallel} = 3.8 \text{\AA}$ in real space, which is approximately the average nearest neighbor distance in the monolayer at the coverage derived above. Consequently, this does not point to an increased buckling. However, only a quantitative analysis of the corrugation function could provide detailed information on the monolayer structure.

5.3.4 Atomic Structure of the Monolayers

In order to illustrate the implications of epitaxy between quasiperiodic materials, a model for the atomic structure of the monolayers on the tenfold surface of Al-Ni-Co is proposed in the following. To derive a suitable model which explains the location of the diffraction spots, some features of the quasiperiodic planes of Al-Ni-Co should be recalled. First, the atoms in the tenfold planes are not only arranged in clusters which are located at the vertices of a random rhombic tiling of 19.79\AA edge length (which was frequently used to explain the structural observations in chapter 4), but they can also be regarded as occupying the majority of the vertices of a rhombic

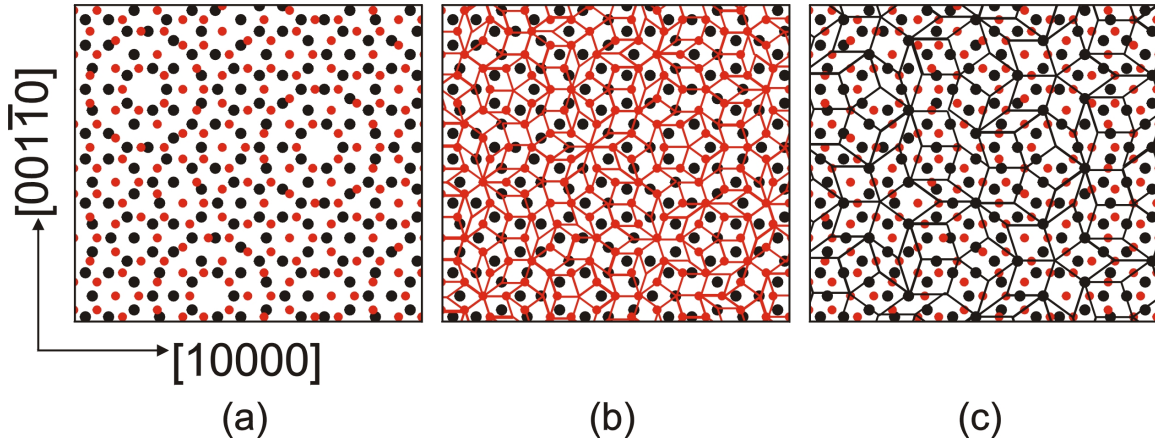


Figure 5.10: (a) Structural model of the clean surface. The red and black circles represent the atoms in the topmost and second layer of the tenfold plane of decagonal Al-Ni-Co. (b) The rhombic tiling on which the atoms of the topmost layer are located. (c) The τ -inflated rhombic tiling indicating the Sb and Bi lattice.

tiling with an edge length of $a_r = 2.456 \text{ \AA}$ (figure 5.10 (b), and [120]). Second, a Penrose tiling and its diffraction pattern are self-similar with a scaling factor of τ . Therefore, from the location of the diffraction spots one cannot decide between tilings scaled by τ . Thus, the first result is that the atoms in the Sb and Bi monolayers are located on a Penrose tiling with an edge length of $2.456\tau^n \text{ \AA}$ with $n = 0, 1, 2, 3, \dots$

The appropriate edge length of the tiling can be found by incorporating the coverage into these structural considerations. The areas of the tiles were given by $A_s = a_r^2 \sin(\pi/5)$ and $A_f = a_r^2 \sin(2\pi/5)$ for the skinny and fat rhombi, respectively (section 2.3). Since the ratio of their frequencies is $1 : \tau$ and each tile is occupied by one atom if all vertices are decorated, the density of atoms ρ in such a tiling is

$$\rho = \frac{1 + \tau}{A_s + \tau A_f} = \frac{1}{a_r^2 \sin \frac{\pi}{5}} \frac{1 + \tau}{1 + \tau^2} . \quad (5.3)$$

The atomic density in a tiling of $a_r = 2.456\tau = 3.974 \text{ \AA}$ leads to $\rho = 0.78 \times 10^{-15} \text{ cm}^{-2}$ which corresponds approximately to the measured coverage.

The placement of the tiling on the substrate can be inferred from the inflation rules illustrated in figure 2.3. The corresponding tiling is shown in figure 5.10 (c). The location of the tiling is such that the atoms are located in high symmetry points of the surface, e.g. in the center of pentagonal arrangements. Moreover, the average distances to the surface layer atoms are maximized.

The monolayer structure just described would yield exactly the observed diffraction spots.

However, this model does not necessarily represent the true atomic arrangement. In order to refine the adsorption sites, a detailed analysis of the LEED intensity as a function of electron energy would be the most promising approach. For this a comparative LEED calculation with experimental data of the clean surface would be a prerequisite. This is already a complex task in itself and is presently worked on in the group of Prof. R. D. Diehl [121]. Further experimental investigations could then lead to an improved structural model of the layers.

5.3.5 Quality of the Quasicrystalline Sb and Bi Films

A striking difference between the spectra of the clean surfaces and the Sb and Bi monolayers on the respective substrate is the distribution of background intensity. The large background intensity around the specular indicates the presence of defects leading to diffuse scattering. In contrast, the background intensity of the monolayers is very low revealing an extremely small density of defects, such as contaminations by residual gas atoms or imperfections in the monolayer. This is in agreement with the results discussed in connection with the thermal stability of the films. While the monolayer is strongly bound to the substrate, atoms in the multilayer easily diffuse during the growth process to reach unoccupied monolayer lattice sites, or desorb if the temperature is sufficiently high. Therefore, a perfect film without defects can be formed. Additionally, the films are inert to contaminations by residual gas atoms in the chamber.

5.4 Coverage beyond the Monolayer

It has already been mentioned that no oscillation of the He specular intensity can be observed with increasing coverage beyond the monolayer, ruling out a layer-by-layer growth mode. The same holds for the intensity of Bragg diffraction peaks. At high coverages, no peaks are observable anymore and also the LEED pattern vanishes. Attempts to obtain an ordered multilayer system by subsequent annealing or simultaneous annealing and deposition of Sb or Bi were not successful. This can be explained by the weak interaction between the adsorbates which does not allow for epitaxially continued multilayers.

5.5 Conclusions

The basic question whether a single element can form an epitaxial quasicrystalline film on quasicrystal surfaces has been resolved. It has been shown that Sb and Bi can form a close-packed monolayer on both the fivefold surface of $\text{Al}_{70.5}\text{Pd}_{21}\text{Mn}_{8.5}$ and the tenfold surface of

$\text{Al}_{71.8}\text{Ni}_{14.8}\text{Co}_{13.4}$. Their coverage corresponds roughly to the Al density in the respective substrate. Probed by electron and helium diffraction, the structure reveals the same Bragg points as the underlying substrate, demonstrating an epitaxial growth mode. The monolayers exhibit an increased corrugation which can be understood by the covalent character of the stabilizing Al-Sb and Al-Bi bonds. The strength of the bonding was investigated by measuring the thermal stability of the films. While the monolayer is strongly bound to the substrate, additional layers desorb at much lower temperature indicating a weak interaction between the adsorbate atoms. For this reason additional layers cannot maintain the quasicrystalline structure. Coverages beyond the monolayers did not yield ordered films.

Finally having found elements which can form quasicrystalline layers, this opens the possibility to study surface characteristics of quasicrystallinity without the impact of a complex alloy composition. For industrial applications surface properties such as the coefficient of friction would be of particular interest, while basic research might focus on atomic growth models.

Having found that Sb and Bi are ideal candidates for quasicrystalline film formation, it might be asked which other elements might be suitable. Early attempts to grow quasicrystalline films concentrated on elements of low surface energy. While this is one essential criterion in order to allow the wetting of the substrate, this requirement is not sufficient as has been shown by gold (Au) [14, 16], aluminum (Al) [9], platinum [109] and silver (Ag) [122] deposition. Even with the influence of indium (In) as a surfactant, Au did not form a quasicrystalline film [15]. As a second condition, a strong bonding to the substrate is essential. Covalent bonds to Al are likely to be established by elements of the fifth group in the periodic table such as Sb and Bi, which were shown here to form quasicrystalline monolayers. It is thus straightforward to study As next. Its deposition will be discussed in the following chapter.